Journal of Pathology
J Pathol 2023
Published online 4 January 2023 in Wiley Online Library
(wileyonlinelibrary.com) DOI: 10.1002/path.6043

ORIGINAL ARTICLE

PARP inhibition promotes endothelial-like traits in melanoma cells and modulates pericyte coverage dynamics during vasculogenic mimicry

Mónica Fernández-Cortés[1], Daniel Delgado-Bellido[1], Eloísa Bermúdez-Jiménez[1], Jesús M Paramio[2], Francisco O'Valle[3], Stefan Vinckier[4], Peter Carmeliet[4,5], Angel Garcia-Diaz[1] and F Javier Oliver[1]*

[1] *Instituto de Parasitología y Biomedicina López Neyra, CSIC, Centro de Investigación Biomédica en Red de Cáncer CIBERONC, Granada, Spain*
[2] *Molecular Oncology Unit, Centro de Investigaciones Energéticas, Medioambientales y Tecnológicas (CIEMAT), Biomedical Research Institute 1+12, University Hospital "12 de Octubre", Centro de Investigación Biomédica en Red de Cáncer (CIBERONC), Madrid, Spain*
[3] *Department of Pathology, Faculty of Medicine, University of Granada (UGR), Granada, Spain*
[4] *Laboratory of Angiogenesis and Vascular Metabolism, Center for Cancer Biology, VIB, & Department of Oncology and Leuven Cancer Institute (LKI), Leuven, Belgium*
[5] *Laboratory of Angiogenesis and Vascular Heterogeneity, Department of Biomedicine, Aarhus University, Aarhus, Denmark*

**Correspondence to: FJ Oliver, Instituto de Parasitología y Biomedicina López Neyra, CSIC, Centro de Investigación Biomédica en Red de Cáncer, CIBERONC, Granada, Spain. E-mail: joliver@ipb.csic.es*

Abstract

Vasculogenic mimicry (VM) describes the ability of highly aggressive tumor cells to develop pseudovascular structures without the participation of endothelial cells. PARP1 is implicated in the activation of hypoxia-inducible factors, which are crucial in tumor neovascularization. We have explored the role of hypoxia and PARP inhibition in VM. In uveal melanoma xenografts, the PARP inhibitor olaparib improved *in vivo* pericyte coverage specifically of VM channels. This was concomitant with reduced metastasis in olaparib-treated VM$^+$ tumors. PARP inhibition and hypoxia modulated melanoma tube formation *in vitro*, inducing a more sparse and regular tubular architecture. Whole-transcriptome profiling revealed that olaparib treatment under hypoxic conditions modulated the expression of genes implicated in vasculogenesis during tube formation, enhancing the endothelial-like phenotype of VM$^+$ uveal melanoma cells. PARP inhibition, especially during hypoxia, upregulated PDGFβ, which is essential for pericyte recruitment. Our study indicates that PARP inhibitors may enhance the endothelial characteristics of VM$^+$ cells, modulate pericyte coverage, and reduce metastatic spread in VM$^+$ melanoma.

Keywords: vasculogenic mimicry; tumor vasculature; PARP inhibitors; olaparib; melanoma; pericytes

Received 10 March 2022; Revised 12 November 2022; Accepted 6 December 2022

No conflicts of interest were declared.

Introduction

Tumor neovascularization is an essential prerequisite for the progression of solid tumors, since it provides the blood supply required to sustain tumor growth. The best-known form of tumor neovascularization is angiogenesis, where new blood vessels sprout from pre-existing vasculature [1]. Angiogenesis was first proposed as a potential therapeutic target in cancer treatment 50 years ago [2], and more than ten different drugs that interfere with vascular endothelial growth factor (VEGF) signaling are now clinically approved for the treatment of several cancer types [3]. However, the clinical benefit of anti-angiogenic therapies is limited, and resistance often arises within a few months. One of the reasons is the appearance of alternative forms of neovascularization, such as vasculogenic mimicry (VM), also known as vascular mimicry. VM, which was first reported by Maniotis *et al* in 1999 [4], is a tumor neovascularization mechanism that does not involve endothelial cells. Instead, VM channels are lined by highly aggressive tumor cells, which acquire molecular traits of endothelial cells, including the expression of a variety of vascular genes. For instance, the aberrant expression of vascular endothelial (VE) cadherin by tumor cells is a frequent hallmark of VM [5]. The presence of VM has been associated with metastasis and poor prognosis in cancer patients [6], but there is currently no way to target VM in clinical settings.

Tumor neovascularization is part of the adaptation of tumor cells to their poorly oxygenated microenvironment, commonly known as tumor hypoxia. Low oxygenation leads to the stabilization of hypoxia-inducible factors (HIFs), which trigger the expression of multiple

genes involved in vascular dynamics, as well as in glucose metabolism, invasion, stemness, and immune evasion, overall favoring malignant transformation [7].

Poly(ADP-ribose) polymerase 1 (PARP1) catalyzes the synthesis and transfer of poly(ADP-ribose) (PAR) to itself or to other target proteins, a process known as parylation. PARP1 has been implicated in the control of many cellular processes. Its crucial role in DNA repair has led to the approval of four different PARP inhibitors (PARPi) for the treatment of homologous recombination-deficient tumors [8]. Moreover, PARP1 has been shown to modulate gene expression in a variety of ways, such as modulating chromatin structure or interacting with sequence-specific transcription factors [9]. We have reported a role for PARP1 in regulating the hypoxia response by modulating HIF-1α [10] and HIF-2α [11]. Given the relevance of hypoxic signaling to VM [5], we hypothesized that the interplay between PARP1 and hypoxia might affect VM formation.

In this study, we have investigated the influence of PARP inhibition and hypoxia on VM in uveal and cutaneous melanoma cells, and we have evaluated the effect of PARPi olaparib on VM^+ and VM^- uveal melanoma xenografts. Our results suggest that PARP inhibition promotes the endothelial-like phenotype of VM^+ melanoma cells, improves pericyte coverage of VM channels *in vivo*, and reduces metastasis in VM^+ melanoma. These findings put forward a new potential target for the control of tumor vasculature that is independent of VEGF signaling, and so could represent an interesting alternative to anti-VEGF therapies in resistant tumors.

Materials and methods

Cell culture

Human uveal melanoma cells Mum2B and Mum2C were cultured in RPMI 1640 medium supplemented with 2 mM L-glutamine, 10% fetal bovine serum, and 1% penicillin/streptomycin (PAA Laboratories, Cölbe, Germany). Human cutaneous melanoma cells SKMEL-147 were cultured in high-glucose DMEM supplemented with 2 mM L-glutamine, 10% fetal bovine serum, and 1% penicillin/streptomycin stock solution (PAA Laboratories). Historical mislabeling of human melanoma cell lines resulted in the publication of a report which reauthenticated Mum2B and Mum2C as C8161 metastatic melanoma cells and OCM-1 uveal melanoma cells, respectively [12]. Taking this into account, we performed a short tandem repeat (STR) analysis for all our human melanoma cell lines, which confirmed the identity of the Mum2B and Mum2C cells used in the present research. Human umbilical vein endothelial cells (HUVECs; Cell Applications, San Diego, CA, USA) were grown in endothelial cell growth medium (Cell Applications/Sigma). Human Retinal Pericytes (Innoprot, Derio, Bizkaia, Spain) were cultured in pericyte medium (Innoprot). All cell lines were cultured in a cell incubator at 37 °C and 5% CO_2. For hypoxic conditions, cells were placed in a sealed hypoxic workstation (Invivo$_2$ 200; Baker Ruskinn, Sanford, ME, USA) in an atmosphere of 1% O_2 and 5% CO_2 at 37 °C. Hypoxic incubation took place for 24 h.

Reagents and antibodies

For *in vitro* experiments, olaparib (Selleckchem, Planegg, Germany) was used at 5 μM for 24 h. For *in vivo* experiments, olaparib (MedChemExpress, Monmouth Junction, NJ, USA) was dissolved in DMSO and further diluted in 10% (2-hydroxypropyl)-β-cyclodextrin (Sigma Aldrich, Darmstadt, Germany) in PBS. Olaparib was administered intraperitoneally at a dose of 50 mg/kg. Treatment with olaparib or vehicle took place three times a week for 3 weeks.

Antibodies and dilutions for tissue immunofluorescence staining were rat CD34 (BD553731; BD Biosciences, Franklin Lakes, NJ, USA), 1:25; rabbit VE-cadherin (ab205336; Abcam, Cambridge, UK), 1:500; mouse S100B (S2532; Sigma Aldrich), 1:100; mouse SMA-Cy3 (C6198; Sigma Aldrich), 1:200; donkey anti-rat immunoglobulin (Jackson Immunoresearch, Ely, UK), 1:200; donkey anti-rabbit immunoglobulin (Jackson Immunoresearch), 1:200; and horse anti-mouse immunoglobulin (Vector Laboratories, Burlingame, CA, USA), 1:100.

Tube formation assay and cell recovery

96-well plate wells were covered with 50 μl of ice-cold growth factor-reduced Matrigel (Corning, Corning, NY, USA), and plates were placed in a cell incubator at 37 °C for 30 min. 10,000 Mum2B or 15,000 SKMEL-147 cells were seeded on Matrigel in the presence of DMSO or 5 μM olaparib. All cells were incubated under normoxia for 1 h before being incubated in normoxia or hypoxia conditions for 24 h. Images were taken on an Olympus CKX41 light microscope (10× objective magnification) coupled to an Olympus E-330 camera (Olympus, Hamburg, Germany). For analysis of gene expression during tube formation assays, 35-mm culture dishes were coated with 770 μl of Matrigel and 380,000 Mum2B cells were seeded on the Matrigel. After a 24-h treatment in the absence or presence of 5 μM olaparib and hypoxia, Mum2B cells were recovered from Matrigel using Cell Recovery Solution (Corning) following the manufacturer's instructions. RNA was extracted from pelleted cells using an RNeasy Mini Kit (Qiagen, Hilden, Germany) following the manufacturer's instructions.

RNA sequencing and data analysis

Library preparation and Illumina sequencing were performed at the Genomics Facility of the Institute for Parasitology and Biomedicine 'López-Neyra' (CSIC, Granada, Spain). Data analysis was performed at the Bioinformatics Facility of the same institute. Total RNA quality was verified using Bioanalyzer RNA 6000 Nanochip electrophoresis (Agilent Technologies,

Santa Clara, CA, USA). All RNA samples showed an RNA integrity number (RIN) value above 9.6. RNA sequencing (RNAseq) libraries were elaborated from 800 ng of input total RNA using a TruSeq Stranded mRNA kit (Illumina, San Diego, CA, USA). A Bioanalyzer high sensitivity DNA assay was performed in order to assess the quality and size distribution of PCR-enriched libraries. Concentration was measured using a Qubit fluorometer (Thermo Scientific, Waltham, MA, USA). Finally, four types of samples (DMSO + normoxia, olaparib + normoxia, DMSO + hypoxia, and olaparib + hypoxia) were sequenced. From each sample type, three biological replicates were made, giving 12 libraries in total. These were pooled in an equimolecular manner and subsequently diluted and denatured following the Illumina NextSeq 500 library preparation guide. The 75 × 2 nt paired-end sequencing was carried out on a NextSeq 500 sequencer, generating an average of 30,059,075 paired reads per sample. Transcriptomes were analyzed using the miARma-Seq pipeline [13]. First, raw sequence data were submitted for evaluation on FastQC software, which provided a thorough report about the quality of the reads [14]. Then the number of reads per sample was homogenized using the software Seqtk [15]. After sample filtering and trimming, a mean of 28,765,495 fragments per sample were obtained with 49% GC content on average. Second, miARma-Seq aligned all processed and quality-filtered sequences using HISAT2 [16], giving a result of 95.86% of adequately aligned reads against *Homo sapiens* Gencode version 26, genome-build GRCh38.p10. In order to obtain expression values, the software featureCounts was used to attribute sequence reads to specific genes [17]. The reference gene annotations were obtained from Gencode from the assembly and genome build indicated above.

Gene enrichment analysis

A functional enrichment study was carried out using the clusterProfiler Bioconductor package [18]. Differentially expressed genes (DEGs) were compared against all expressed genes in the RNAseq assay. Gene ontology terms for each gene were obtained from the Bioconductor *Homo sapiens* database and were associated with Entrez gene identifiers in an orgDB R object through the AnnotationForge package to be used with clusterProfiler. Gene ontology enrichment analysis was performed for Biological Process, Molecular Function, and Cellular Complex terms. KEGG enrichment was also calculated from *Homo sapiens* gene names previously acquired from Gencode. A gene set enrichment analysis (GSEA) was performed between DMSO + normoxia and olaparib + hypoxia samples [19]. Gene sets from the Molecular Signatures database (MSigDB) v6.2 were used for GSEA [KEGG: 186 canonical pathways from the Kyoto Encyclopedia of Genes and Genomes (KEGG) pathway database; C5: 825 gene sets based on the gene ontology term]. Default parameters were used to identify significantly enriched gene sets [false discovery rate (FDR) $q < 0.25$].

RT-qPCR

500,000 Mum2B or 600,000 SKMEL-147 cells were seeded in 60-mm culture dishes and incubated overnight. Cells were treated with DMSO or olaparib at 5 μM and incubated in normoxia or hypoxia conditions for 24 h. Total RNA was extracted using an RNeasy Mini Kit (Qiagen) following the manufacturer's instructions. RNA extracts were subjected to a digestion step with DNAse I (Invitrogen, Waltham, MA, USA) and reverse-transcribed using iScript Reverse Transcription Supermix (BioRad, Hercules, CA, USA) according to the manufacturer's instructions. Target sequences were amplified with iTaq Universal SYBR Green Supermix (BioRad) using the following primers: *CDH5* forward 5'-AACTTCCCCTTCTTCACCC-3', *CDH5* reverse 5'-AAAGGCTGCTGGAAAATG-3', *NRP1* forward 5'-AAAACGGTGCCATCCCT-3', *NRP1* reverse 5'-AAGAAGCAGAGTGGGTCGTT-3', *TIE1* forward 5'-GTGCCACCATTTTGACACTG-3', *TIE1* reverse 5'-CAGGCACAGCAGGTTGTAGA-3', *PDGFB* forward 5'-CATTCCCGAGGAGCTTTATG-3', *PDGFB* reverse 5'-CTCAGCAATGGTCAGGGAAC-3', 36B4 forward 5'-CAGATTGGCTACCCAACTGTT-3', and 36B4 reverse 5'-GGCCAGGACTCGTTTGTACC-3', where 36B4 was used as a positive and normalization control.

Enzyme-linked immunosorbent assay (ELISA)

200,000 Mum2B cells were seeded in the wells of a six-well plate and incubated overnight. Cells were treated with DMSO or olaparib at 5 μM and incubated in normoxia or hypoxia conditions for 24 h. Conditioned media were recovered and concentrated using Amicon Ultra-2 centrifugal filter units (Millipore, Burlington, MA, USA) with a 10 kDa nominal molecular weight cut-off. ELISA was performed using the commercial human PDGF-BB Mini ABTS ELISA Development Kit (PeproTech, London, UK), following the manufacturer's instructions.

siRNA-mediated knockdown

PDGFB expression was knocked down with predesigned siRNA SASI_Hs01_00121961 and SASI_Hs01_00121962 (Sigma Aldrich), which were co-transfected. As a negative control, we used a scrambled siRNA (Sigma Aldrich): 5'-CUUUGGGUGAUCUACGUUA[dT]-3'. siRNAs were transfected using the transfection reagent jetPRIME (Polyplus, Illkirch, France) following the manufacturer's instructions.

Cell migration assay

Pericyte migration in the presence of Mum2B-conditioned media was assessed *in vitro* using 6.5-mm Transwell inserts with an 8.0-μm pore size (Costar,

Corning). In brief, 150,000 Mum2B cells were seeded in six-well plates and transfected with scrambled or siPDGFB siRNA. After 24 h, transfection medium was replaced with fresh growth medium containing DMSO or olaparib. Conditioned media were collected 24 h later and placed in the lower chamber of Transwell plates. Recombinant human PDGF-BB (PeproTech) was added at 1 ng/ml as a positive control for pericyte migration; 8,000 retinal pericytes were placed on the upper chamber of the Transwell and allowed to migrate for 6 h. Transwell inserts were then washed in PBS and non-migrated pericytes were removed from the upper side of the Transwell with a wet cotton swab. Inserts were fixed in 4% paraformaldehyde solution (ChemCruz, Dallas, TX, USA) for 15 min and washed in PBS. Inserts were then stained with crystal violet (Sigma Aldrich) for 30 min and washed in PBS. Images of migrated pericytes were taken on an Olympus CKX41 light microscope (10× objective magnification) coupled to an Olympus E-330 camera (Olympus).

Human uveal melanoma xenografts

Five-week-old female Swiss nude mice received a subcutaneous injection of 4,000,000 VM^+ Mum2B or VM^- Mum2C cells in 100 µl of PBS. Tumor volumes were measured using a caliper and applying the formula $V = \pi \times [D \times d^2]/6$, where D is the major tumor axis and d is the minor tumor axis. Once tumors grew to approximately 100 mm^3, tumor-bearing mice were randomized for further treatment with vehicle or olaparib (50 mg/kg, intraperitoneal) three times a week for 3 weeks. Mice were then anesthetized and perfused with saline followed by 4% paraformaldehyde via intracardiac injection. Internal organs were examined to detect the presence of metastasis. The experimental protocols of this study conform to European Union Directive 2010/63 and followed the ethical guidelines for investigations with experimental animals approved by the Ethics Review Committee for Animal Experimentation of the Spanish Council of Scientific Research. These procedures were performed at the Animal Facility at the Institute for Parasitology and Biomedicine 'López-Neyra' (CSIC, Granada, Spain). Local and metastatic tumors were harvested, fixed in formalin, and embedded in paraffin by Dr Francisco O'Valle's group (Anatomical Pathology Department, University of Granada). Tumor samples were then sectioned at 7-µm thickness at the Histology unit of Dr Peter Carmeliet's research group.

Tumor hypoxia

In order to assess *in vivo* tumor hypoxia, pimonidazole hydrochloride (Cayman Chemical Company, Ann Arbor, MI, USA) was dissolved in vehicle and injected intraperitoneally in tumor-bearing mice at 60 mg/kg 60 min before sacrifice. Hypoxic pimonidazole adducts were detected with Hypoxyprobe1-Mab1 (Chemicon, Temecula, CA, USA), following the instructions provided by the manufacturer. The staining was performed by the Histology team of Dr Peter Carmeliet's research group. Images were acquired using a Leica DMI6000 B microscope (Leica Microsystems, Wetzlar, Germany).

Image analysis

Tube formation images from Mum2B and SKMEL-147 cells (at least three images per condition) were analyzed using the online software WimTube (Wimasis, Onimagin Technologies, Córdoba, Spain), which quantifies a number of parameters of tubular networks, namely covered area, branching points or tube length, among others.

Images of Transwell inserts (at least three images per insert) were analyzed using Fiji [20]. The amount of transmigrated pericytes was quantified as the area with positive staining for crystal violet.

Images from tumor CD34/VE-cadherin/α-smooth muscle actin (αSMA) staining (ten random optical fields per tumor section, more than five tumors per experimental group) were analyzed using Fiji. A threshold for $CD34^+$, VE-$cadherin^+$, and αSMA^+ staining was established independently. VM formation was assessed as the ratio between total $CD34^+$ staining and total VE-$cadherin^+$ staining. $CD34^+$/VE-$cadherin^+$ structures were classified as endothelial vessels, whereas $CD34^-$/VE-$cadherin^+$ structures were classified as VM channels. The integrity of intercellular contacts was quantified as the percentage of VE-$cadherin^+$ area within the total vessel area. Pericyte coverage was determined as the percentage of vessel perimeter that was positive for αSMA staining.

Statistical analyses

All data from *in vitro* results (RT-qPCR, tube formation parameters, etc.; $n \geq 3$) were subjected to two-tailed Student's *t*-test or ANOVA analysis. Results are shown as mean ± SEM. Data from tumor volumes and tumor hypoxia ($n \geq 5$) were subjected to ANOVA analysis. Results are shown as median ± interquartile range. Regarding tumor metastasis ($n \geq 5$), metastasis-positive mice were assigned a value of 1, while metastasis-negative mice were assigned a value of 0. Data were subjected to ANOVA analysis. Data from pericyte coverage were analyzed using Mann–Whitney two-tailed tests. Results are shown as median ± 90% confidence interval.

Results

The combination of olaparib plus hypoxia enhances vasculogenic gene expression in VM^+ uveal melanoma cells during tube formation

We aimed to find out whether hypoxia or PARP inhibition could modulate the expression of genes involved in vascular dynamics in VM^+ tumor cells. We cultured the highly aggressive uveal melanoma cell line Mum2B on Matrigel in order to trigger capillary-like tube formation [4,21], and treated the cells with DMSO or 5 µM

olaparib in normoxic or hypoxic (1% O_2) conditions. After 24 h, when tubular networks were established, total RNA was extracted for whole-transcriptome profiling (supplementary material, Table S1). In these conditions, the resulting transcriptome represents gene expression taking place during tube formation.

Treatment with olaparib significantly changed the expression of 596 genes (supplementary material, Figure S1A), hypoxia significantly modulated 1,897 genes (supplementary material, Figure S1B), while treatment with olaparib plus hypoxia resulted in a significant change in the expression of 4,780 genes (supplementary material, Figure S1C), compared with normoxic controls (FDR < 0.05). We examined side by side the genes that were significantly modulated by olaparib and hypoxia alone or in combination, with reference to normoxic controls (supplementary material, Figure S1D). Remarkably, 2,859 genes were significantly modulated only by the combination of olaparib plus hypoxia (supplementary material, Table S1).

GSEA did not identify global modulation of any pathways related to vascular function after olaparib treatment or hypoxia alone. However, GSEA highlighted a total of 12 gene ontology terms related to vessel formation that were globally altered in the olaparib plus hypoxia condition, compared with untreated normoxic controls (Figure 1A–C and supplementary material, Figure S2 and Table S2). Overall, GSEA detected 140 genes implicated in vascular biology whose expression was significantly upregulated in this condition (supplementary material, Table S2, Sheet1), suggesting a promotion of the vasculogenic gene expression profile. Among these, we found a number of genes with crucial roles in endothelial and vascular development, such as *VEGFA/B/C*, *PECAM1*, *RHOJ*, *CD34*, *PDGFB*, *CDH5*, *ROBO4*, *KDR* (VEGFR2), *NRP1/2*, *PTPRB* (VE-PTP), or *TIE1* [1,22,23].

We validated the RNAseq results for some vasculature-related genes in Mum2B (Figure 1D) and also in the cutaneous melanoma cell line SKMEL-147 (Figure 1E). The expression of *PECAM1* and *CD34* could not be detected by RT-qPCR in either cell line, but we measured the expression of *CDH5*, *NRP1*, *TIE1*, and *PDGFB*. Consistent with the RNAseq data, all of these genes were significantly upregulated by olaparib plus hypoxia in Mum2B, compared with normoxic controls, and in some cases by olaparib or hypoxia alone. In SKMEL-147, the expression of vascular genes was lower (*TIE1* expression could not be detected), but the expression of *CDH5* and *PDGFB* was significantly upregulated by olaparib plus hypoxia as well. Protein expression of PDGFβ was further validated by ELISA (Figure 1F), measuring its concentration in Mum2B-conditioned media. PDGFβ secretion was significantly increased by olaparib during both normoxia and hypoxia. As a reference for gene expression in endothelial cells, we also measured gene expression in HUVECs (Figure 1G). Interestingly, we found that olaparib and hypoxia had the opposite effect on the expression of *CDH5*, *NRP1*, and *TIE1* in endothelial cells, with all three being significantly downregulated after combined treatment. However, the expression of *PDGFB* did not undergo any significant changes in HUVECs.

PARP inhibition and hypoxia modulate melanoma tube formation on Matrigel

In order to assess whether treatment with PARPi and hypoxia had an effect on the tube formation ability of VM^+ melanoma cells, we cultured Mum2B (Figure 2) and SKMEL-147 (supplementary material, Figure S3) on Matrigel in the absence or presence of PARPi and hypoxia and analyzed tube formation parameters. We also analyzed tube formation parameters in the same conditions in HUVECs (supplementary material, Figure S4), as an endothelial control.

In Mum2B, olaparib or hypoxia alone (Figure 2A, second and third panels) did not seem to have any major effect on tube formation. Nevertheless, combined treatment with olaparib during hypoxia (Figure 2A, fourth panel) affected the overall morphology of the tubular networks, which now appeared more regular and presented a better tube structure. Quantitatively (Figure 2B–D), treatment with olaparib during hypoxia significantly reduced the covered area, total branching points, and total tube length. There was also a significant gain in the loop area (the empty spaces between tubes), meaning that tubes were more dispersed. Altogether, these changes represent a reduction in the density of tubular networks, and a network morphology that evokes vessel normalization. Tube formation assays in SKMEL-147 provided very similar results (supplementary material, Figure S3): the combination of olaparib plus hypoxia caused a significant decrease in the covered area, total branching points, total loops, and total tube length. An increase in the mean loop area seemed to take place too, though it was not statistically significant. Still, the changes detected after olaparib plus hypoxia in SKMEL-147 also reveal a reduction in the density of tubular networks, and this reduction was also accompanied by a visible improvement in tube structure.

As seen for gene expression, olaparib and hypoxia exerted the opposite effect on tube formation by HUVECs (supplementary material, Figure S4). In these cells, olaparib plus hypoxia significantly increased the number of branching points, loops, and total tube length, while the mean loop area was significantly reduced.

Taking the above results together, we have shown that PARP inhibition and hypoxia, especially in combination, can enhance endothelial-like gene expression and favor a structural normalization of tubular networks in VM^+ melanoma cells. In HUVECs, however, PARP inhibition during hypoxia decreased the expression of several endothelial genes (*CDH5*, *NRP1*, and *TIE1*, but not *PDGFB*), while increasing the density of tubular networks on Matrigel. These findings suggest that the regulation of endothelial-like characteristics is different in melanoma cells compared with primary endothelial cells.

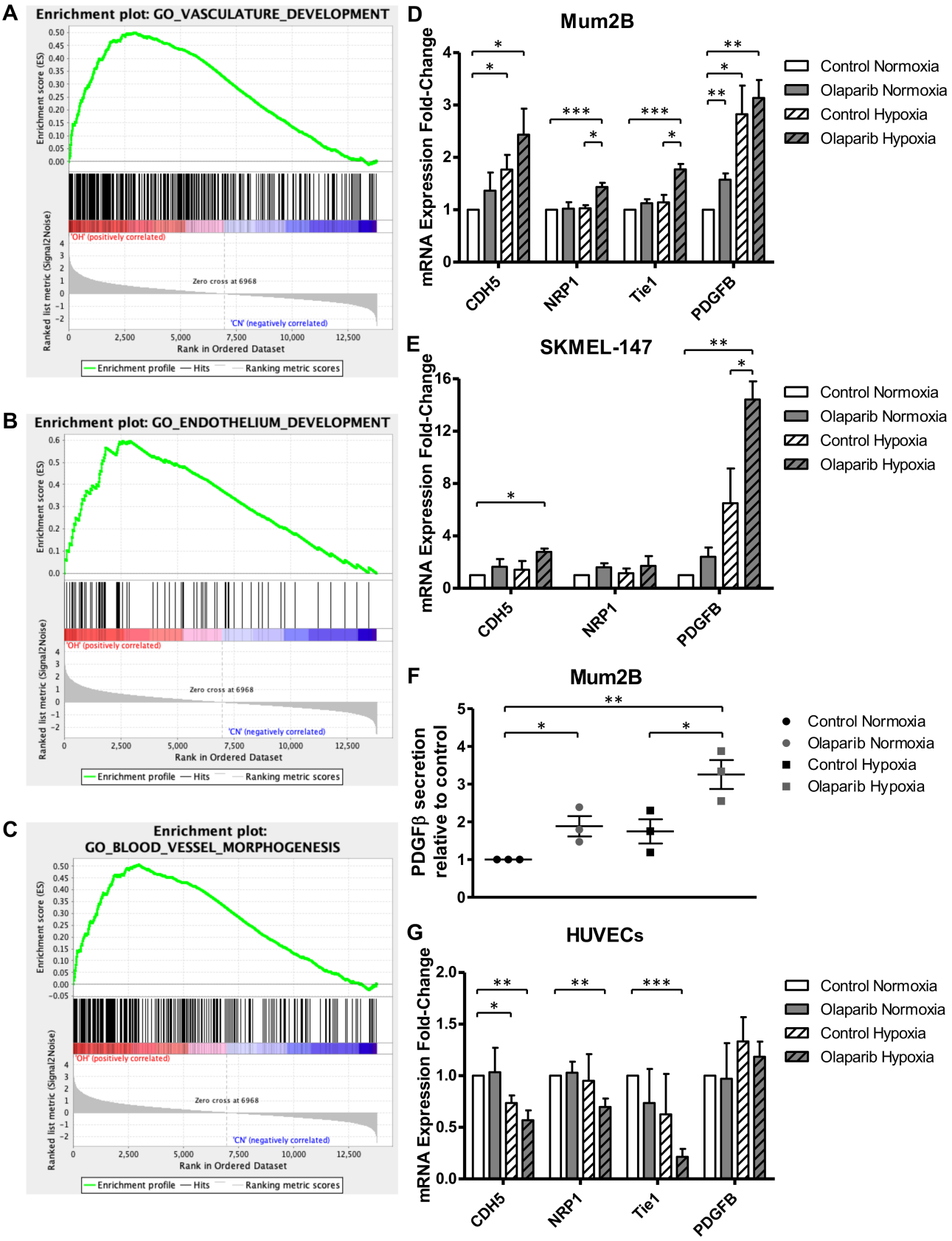

Figure 1. The combination of PARP inhibition plus hypoxia modulates vasculogenic gene expression in VM^{+} melanoma cells. (A–C) RNAseq data comparing gene expression after olaparib plus hypoxia with normoxic controls were subjected to GSEA and enrichment plots were generated. (D) Mum2B, (E) SKMEL-147, and (G) HUVECs were treated with DMSO or olaparib and incubated under normoxia or hypoxia for 24 h. Total RNA was extracted and gene expression was measured using RT-qPCR. (F) Mum2B cells were treated with DMSO or olaparib and incubated under normoxia or hypoxia for 24 h, and the concentration of PDGFB in conditioned media was measured using ELISA. *$p < 0.05$; **$p < 0.01$; ***$p < 0.001$ (Student's t-test, $n \geq 3$).

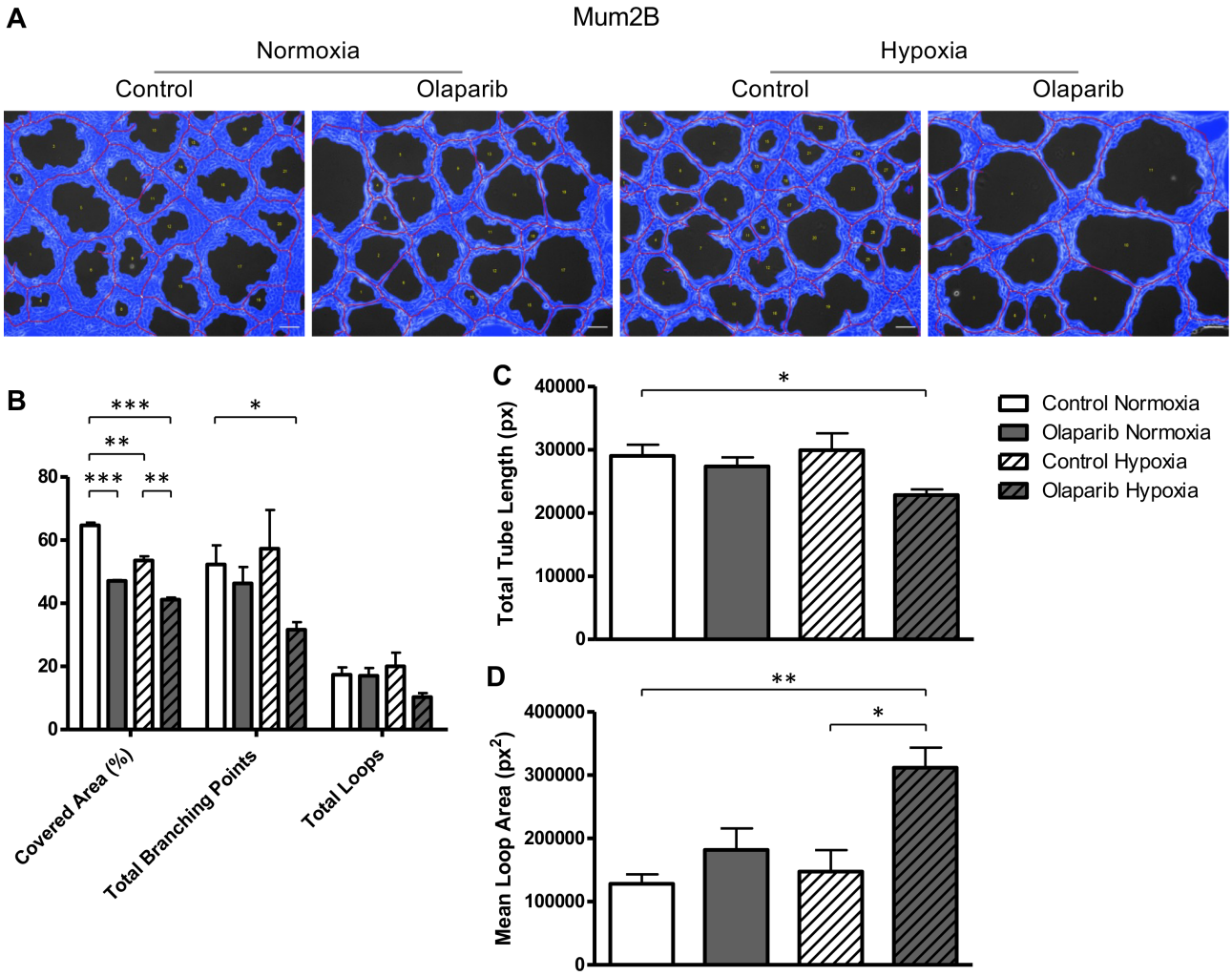

Figure 2. PARP inhibition and hypoxia modulate tube formation by VM^+ uveal melanoma cells. (A) Mum2B cells were cultured on Matrigel in the absence or presence of olaparib and incubated under normoxia or hypoxia for 24 h. (B–D) Tube formation parameters (covered area, branching points, loops, tube length, and loop area) were quantified using the image analysis software WimTube (Wimasis). *$p < 0.05$; **$p < 0.01$; ***$p < 0.001$ (Student's *t*-test, $n \geq 3$). Scale bar: 100 µm.

Olaparib treatment favors pericyte migration *in vitro* in a PDGFβ-dependent manner

PDGFβ reportedly triggers pericyte recruitment towards endothelial vessels [24]. We hypothesized that increased PDGFβ expression (Figure 1D,E) and secretion (Figure 1F) in melanoma cells after olaparib treatment might entail changes in pericyte behavior. We knocked down *PDGFB* expression (supplementary material, Figure S5) in Mum2B in the absence and presence of olaparib and subsequently performed Transwell migration assays in order to evaluate the ability of Mum2B-conditioned medium to stimulate pericyte migration *in vitro* (Figure 3).

Conditioned medium of olaparib-treated Mum2B cells significantly increased pericyte migration compared with control conditioned medium. However, this increase did not take place when *PDGFB* expression was knocked down. The addition of exogenous PDGFβ to the conditioned medium restored the increase in pericyte migration.

These results show that olaparib treatment can enhance the ability of uveal melanoma cells to recruit pericytes *in vitro* and that this recruitment depends on the expression of PDGFβ.

Olaparib affects the incidence of metastasis in VM^+ tumors

We generated human uveal melanoma xenografts using the cell lines Mum2B and Mum2C. The poorly aggressive cell line Mum2C was used as a negative control for VM formation (supplementary material, Figure S6A) [25]. Tumor-bearing mice were treated with olaparib (50 mg/kg) or vehicle in order to explore the effect of PARP inhibition on the progression of VM^+ and VM^- tumors.

Final tumor size was similar in all the experimental groups, with no significant effect that could be attributed to treatment or to the different cell lines (Figure 4A). However, careful examination of internal organs revealed a variation in the incidence of metastasis (Figure 4B). In particular, olaparib treatment significantly reduced the incidence of metastasis in Mum2B-bearing mice. Furthermore, treatment with olaparib

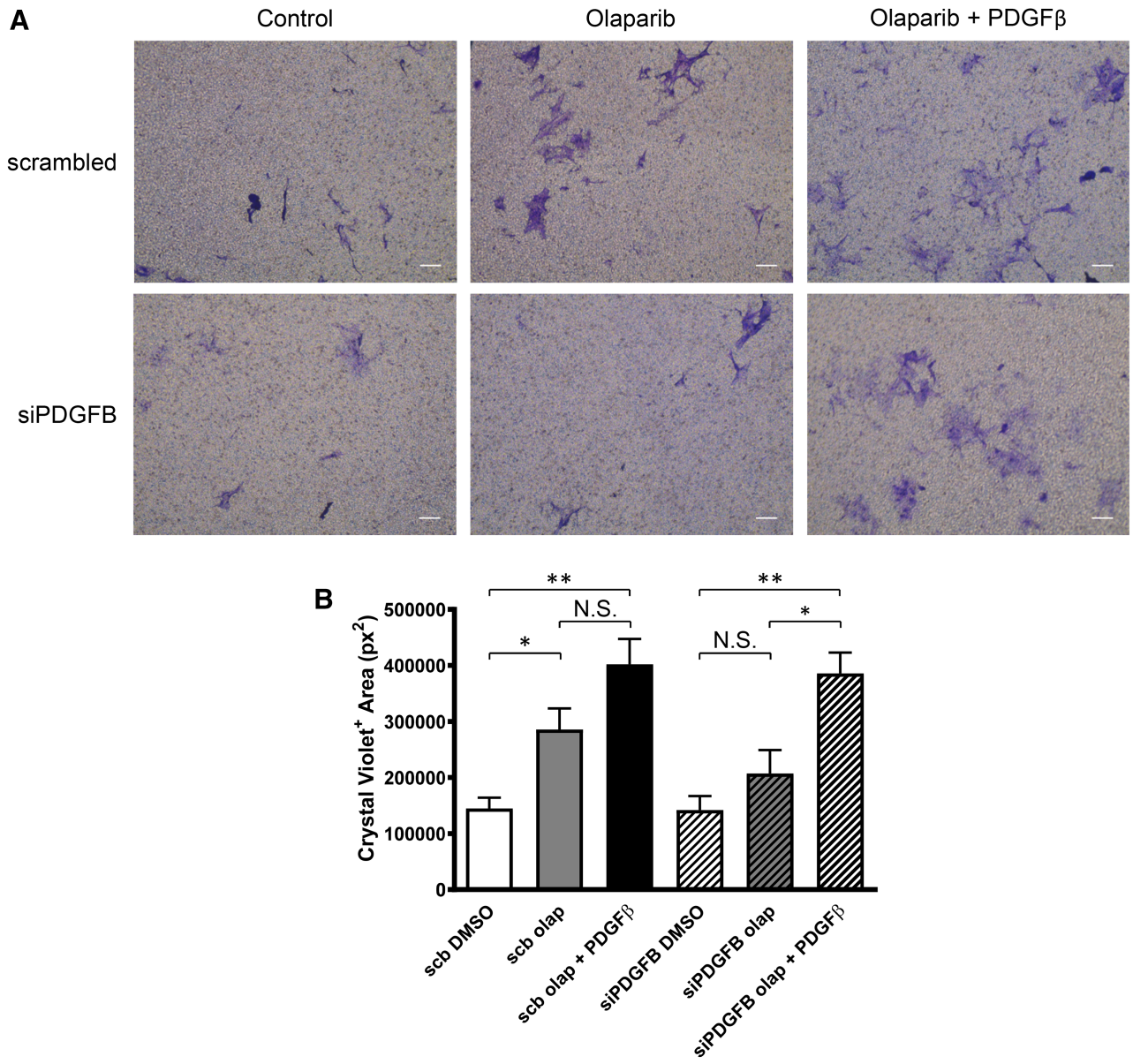

Figure 3. PARP inhibition increases pericyte migration *in vitro* in a PDGFB-dependent manner. (A) Mum2B cells with PDGFB expression knocked down were treated or not with olaparib. Conditioned medium was placed in the lower chamber of Transwell plates. Human PDGFβ was added as a positive control for pericyte migration. Human retinal pericytes were placed on the upper chamber of Transwell plates and allowed to migrate for 6 h. Migrated pericytes were stained with crystal violet. (B) Migrated pericytes were quantified using Fiji as the area with positive staining by crystal violet. N.S., not significant. *$p < 0.05$; **$p < 0.01$ (Student's *t*-test, $n = 3$). Scale bar: 100 μm.

seemed to affect not only the presence of metastasis but also the size of metastatic tumors (supplementary material, Figure S6B); the only metastasis found in Mum2B-bearing mice treated with olaparib was considerably smaller than metastases found in mice treated with vehicle. All metastases in the different groups were found in the peritoneal cavity.

Endothelial and VM vessels *in vivo*

The presence of VM *in vivo* was determined through CD34/VE-cadherin/S100B co-immunofluorescence staining (supplementary material, Figure S6C,D), where CD34 was used as an endothelial-specific marker, VE-cadherin as a dual marker for endothelial vessels and VM pseudovessels, and S100B as a melanoma cell marker [26]. Therefore, $CD34^+$/VE-$cadherin^+$/$S100B^-$ vessels are genuine endothelial vessels, while $CD34^-$/VE-$cadherin^+$/$S100B^+$ structures represent VM channels. As expected, VM was observed in Mum2B- (supplementary material, Figure S6C, arrows) but not Mum2C-derived (supplementary material, Figure S6D) tumors. We quantified total $CD34^+$ and VE-$cadherin^+$ staining independently in all tumor samples. The ratio between CD34 and VE-cadherin staining (supplementary material, Figure S6E) was considered a measure for the overall presence of VM. Indeed, the CD34/VE-cadherin ratio was significantly higher in Mum2C

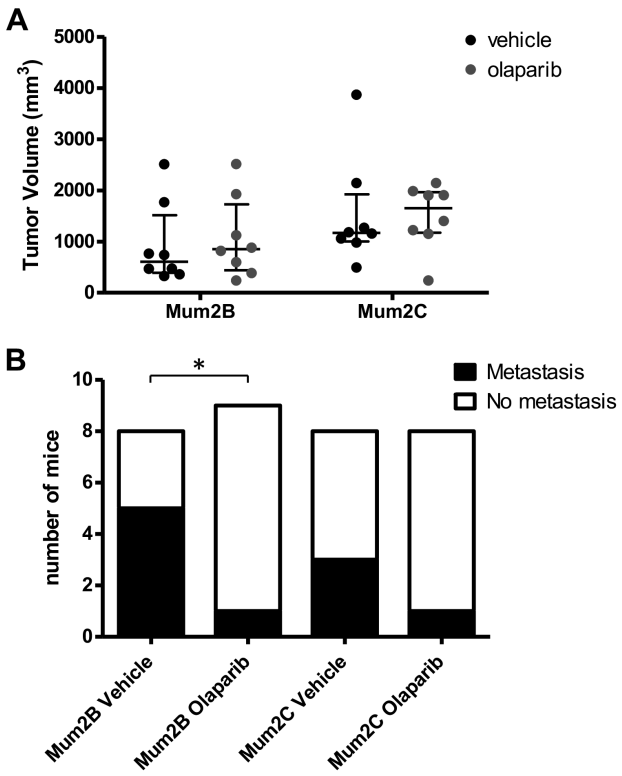

Figure 4. PARP inhibition affects the incidence of metastasis in VM^+ uveal melanoma xenografts. Human subcutaneous uveal melanoma xenografts were generated in immunocompromised mice, which were treated with vehicle or olaparib (50 mg/kg) for 3 weeks. (A) Final tumor volume was measured with a caliper in all mice before sacrifice. There were no significant differences among the different experimental groups. (B) Upon sacrifice, mice were dissected and examined for the presence of metastasis. *$p < 0.05$ (Student's *t*-test, $n \geq 8$).

tumors, where there are no $CD34^-$/VE-cadherin$^+$ structures. Olaparib did not alter the CD34/VE-cadherin ratio in any case, suggesting that PARP inhibition does not affect the overall ability to develop VM structures.

Our *in vitro* results suggest that olaparib may have a deeper effect on the vasculogenic phenotype under hypoxic conditions, so we evaluated the oxygenation status of the tumor xenografts (supplementary material, Figure S6F). As expected in solid tumors, all samples showed $PIMO^+$ staining, revealing the presence of hypoxic regions.

PARP inhibition has opposing effects on pericyte recruitment to endothelial versus VM vessels *in vivo*

As discussed above, PARP inhibition promoted the expression and secretion of PDGFβ in VM^+ melanoma cells (Figure 1D–F), as well as their ability to stimulate pericyte migration *in vitro* (Figure 3). We hypothesized that this might influence pericyte recruitment to vascular and pseudovascular structures *in vivo*. In order to explore this possibility, tumor sections were stained for CD34, VE-cadherin, and the mural cell marker αSMA [27] (Figure 5 and supplementary material, Figure S7). In this model, CD34/VE-cadherin/αSMA co-localization can be considered as pericyte coverage in endothelial vessels, while $CD34^-$/VE-cadherin$^+$/αSMA$^+$ staining indicates pericyte coverage in VM pseudovessels.

Examination of Mum2B tumor sections (Figure 5) confirmed an association of pericytes with VM channels *in vivo* (Figure 5, gold arrow), supporting the observations of Thijssen *et al* [28]. Considering all vessel types, global pericyte coverage in Mum2B-derived tumors did not seem to vary between olaparib- and vehicle-treated mice (Figure 5C). However, significant differences could be detected when analyzing endothelial and VM vessels separately. In the case of $CD34^+$/VE-cadherin$^+$ endothelial vessels (Figure 5E), pericyte recruitment was reduced after olaparib treatment. Surprisingly, we observed the opposite outcome for VM $CD34^-$/VE-cadherin$^+$ pseudovessels (Figure 5D), where olaparib significantly increased pericyte coverage, consistent with our *in vitro* results concerning PDGFβ and pericyte migration. We did not find any significant differences in PDGFB after hypoxia or olaparib treatment in HUVECs (Figure 1G); thus, the decrease in pericyte recruitment to endothelial vessels must be due to other causes. Interestingly, in VM^- Mum2C-derived tumors (supplementary material, Figure S7), pericyte coverage of endothelial vessels was significantly higher after olaparib treatment (supplementary material, Figure S7C). This suggests that the effect of olaparib on pericyte recruitment is different in VM^+ and VM^- tumors; olaparib improves the pericyte coverage of endothelial vessels in the absence of VM (Mum2C-derived tumors), but it selectively improves the pericyte coverage of VM channels when they are present (Mum2B-derived tumors).

Thus, PARP inhibition increased pericyte recruitment specifically to VM pseudovessels, which may have implications in pseudovessel maturation and function.

Discussion

Alternative neovascularization mechanisms, such as VM, have been gaining attention in recent years. This interest has been motivated by the limitations encountered by anti-angiogenic therapies. Several reports have shown a positive correlation between anti-angiogenic treatments, such as bevacizumab, and VM formation [29,30], suggesting that VM can arise as an adaptive response to enable tumor perfusion and elicit resistance. Many important genes in endothelial and VM development are direct targets of HIFs, making tumor hypoxia a critical initiator of angiogenesis as well as VM [5,7]. In turn, we have reported a role for PARP1 in modulating the hypoxia response by modulating HIF1α [10] and HIF2α [11], which prompted us to explore the interplay between VM, hypoxia, and PARP inhibition.

Our '-omics' approach to understanding the role of PARPi and hypoxia in the modulation of VM led to the identification of thousands of genes that were regulated by these conditions during tube formation *in vitro*. Interestingly, the combination of olaparib plus hypoxia

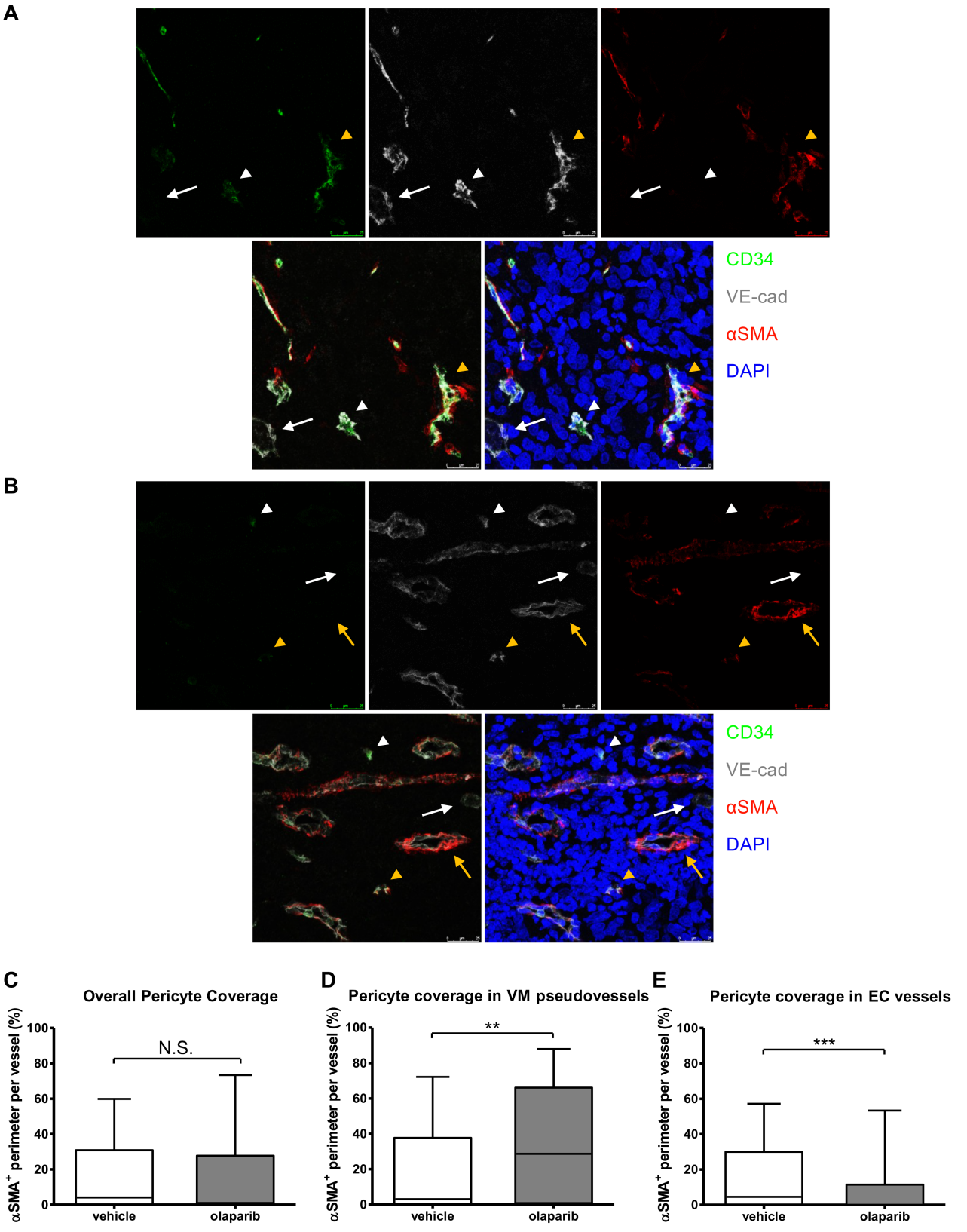

Figure 5. PARP inhibition has opposing effects on pericyte recruitment to endothelial vessels and VM channels *in vivo*. (A) Vehicle- and (B) olaparib-treated Mum2B-derived tumor sections were co-immunostained for CD34, VE-cadherin, and αSMA. Arrows: $CD34^{-}$/VE-$cadherin^{+}$ VM channels. Arrowheads: $CD34^{+}$/VE-$cadherin^{+}$ endothelial vessels. White arrows/arrowheads: not covered by pericytes (SMA^{-}). Gold arrows/arrowheads: covered by pericytes (SMA^{+}). Pericyte coverage in tumor vasculature was measured using Fiji as the percentage of (C) VE-$cadherin^{+}$, (D) $CD34^{+}$/VE-$cadherin^{+}$, or (E) $CD34^{-}$/VE-$cadherin^{+}$ vessel perimeter that co-localized with αSMA ($n \geq 398$, $n \geq 71$, and $n \geq 307$ vessel structures per experimental group, respectively). N.S., not significant. $^{**}p < 0.01$; $^{***}p < 0.001$ (two-tailed Mann–Whitney test, ≥5 mice per experimental group). Scale bar: 25 μm. EC, endothelial cell.

resulted in the significant modulation of over 2,000 genes that were not modulated by olaparib or hypoxia alone. This suggests that there must be some sort of additive or synergistic interaction between olaparib treatment and the hypoxia response regarding the regulation of gene expression.

GSEA highlighted the upregulation of 140 genes implicated in endothelial and vascular biology, indicating that the combination of olaparib and hypoxia may enhance the endothelial-like phenotype of VM^+ tumor cells. The fact that olaparib and hypoxia collectively modulate such a high number of vasculature-related genes suggests that they might affect the activity of one or a few master regulators of endothelial gene expression. In a recent report, we found that olaparib upregulated long non-coding RNAs (lncRNAs) that were predicted targets of the transcription factor ETS1 [31], in line with previous findings showing increased ETS1 transcriptional activity after PARP inhibition [32]. ETS1 has been extensively reported to modulate endothelial function [33–36], making it an interesting candidate for further research in VM regulation.

Notably, the effect of olaparib plus hypoxia on gene expression is different in VM^+ melanoma cells and in HUVECs. Indeed, most of our results show opposing effects of olaparib on VM and endothelial cells, hinting at a cell type-specific mechanism. We could hypothesize that the behavior of tumor cells may differ due to the deregulation of regulatory mechanisms that support the pluripotency of these highly aggressive cells [37].

PDGFβ has a crucial role in pericyte recruitment towards endothelial vessels [24] as well as VM channels [28]. We have shown that PDGFβ expression and secretion were upregulated by olaparib in VM^+ melanoma cells but not in HUVECs. Upregulated PDGFβ secretion in uveal melanoma cells after olaparib treatment enhanced their ability to stimulate pericyte migration *in vitro*. Indeed, our *in vivo* experiments demonstrated a significant increase in pericyte coverage of VM channels in olaparib-treated mice, showing a promotion of pericyte recruitment.

Surprisingly, olaparib treatment had opposing effects on pericyte coverage of endothelial vessels, which was reduced in VM^+ tumors but increased in VM^- tumors. This indicates that the presence or absence of VM influences vascular dynamics within the tumor. Focusing on VM^+ tumors, overall pericyte coverage was not affected by olaparib treatment, meaning that the total number of pericytes associated with tumor vasculature did not change in response to olaparib. Hence, the observed changes could represent a shift in the pericyte population towards VM channels and away from endothelial vessels, due to increased PDGFβ secretion specifically by VM cells. In other words, there might be a competition between endothelial and VM vessels for the recruitment of the pericytes available within the tumor, and olaparib could tip the balance in favor of VM channels by upregulating PDGFβ. In contrast, this competition would not take place in VM^- tumors, so pericyte coverage would not decrease in response to olaparib. On the contrary, olaparib promoted pericyte coverage of endothelial vessels in VM^- tumors. Riedel *et al* reported that the anti-cancer agent RAPTA-T, which seemingly reduced PARP activity, could increase pericyte coverage in mesothelioma xenografts, and this increase correlated with reduced poly(ADP) ribose [38].

We show that olaparib can reduce metastatic spread specifically in Mum2B-derived tumors, an effect that we attribute to the modulation of VM. The promotion of endothelial gene expression, the improved tube structure as seen *in vitro*, plus the stabilizing action of pericytes *in vivo* after olaparib treatment may lead to some degree of 'pseudovessel maturation' of VM channels. This could in turn hinder tumor cell intravasation and hence metastasis, similarly to the effect reported for the normalization of endothelial vasculature [39]. In fact, we show reduced metastasis in response to olaparib even if it appears to contribute to the abnormalization of endothelial vessels, which show reduced pericyte coverage and weaker intercellular contacts in VM^+ tumors. This highlights the relevance of targeting not only endothelial vessels but also VM channels in cancer therapy.

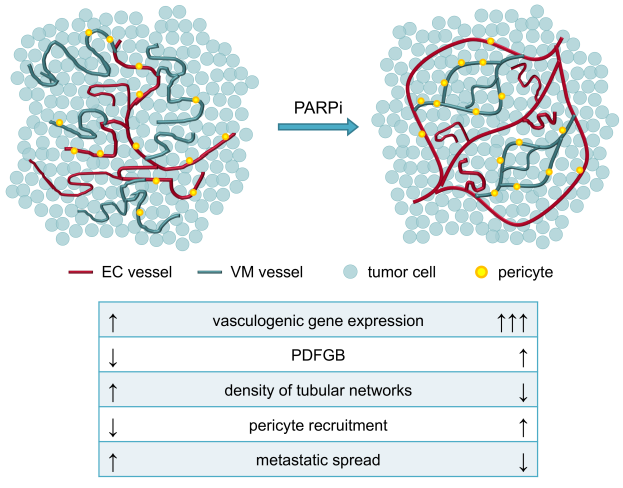

Figure 6. PARP inhibition modulates VM in melanoma. PARP inhibition and hypoxia induce pro-vasculogenic gene expression in VM^+ melanoma cells, including an upregulation of PDGFβ. This may favor a partial maturation of VM pseudovessels, as illustrated by increased pericyte recruitment *in vivo*. These changes were concomitant with reduced metastasis in VM^+ tumors. EC, endothelial cell.

Conclusions

In summary (Figure 6), our study reveals a role for PARP inhibition in the regulation of melanoma VM *in vitro* and *in vivo*. *In vitro*, the PARP inhibitor olaparib in the presence of hypoxia enhanced the endothelial-like phenotype of VM^+ melanoma cells during tube formation, while modulating tubular network architecture. *In vivo*, olaparib affected pericyte coverage dynamics, favoring pericyte recruitment to VM channels, which was concomitant with a decrease in the incidence and size of metastatic VM^+ tumors.

Acknowledgements

RNA sequencing and bioinformatics analyses were carried out at the Instituto de Parasitología y Biomedicina 'López-Neyra' (IPBLN-CSIC) in the Genomics and Bioinformatics Units. This work was supported by the Spanish Ministry of Economy and Competitiveness and the Spanish Ministry of Science and Innovation, SAF2015-70520-R, RTI2018-098968-B-I00, RTICC RD12/0036/0026, and CIBER Cáncer ISCIII CB16/12/00421; a grant from Junta de Andalucía, PY20_01179; and Fundación Domingo Martínez to FJO.

Author contributions statement

MFC performed the experiments, contributed to their design, and wrote the article. DDB performed experiments and discussed the results. EBJ performed experiments. JMP discussed the results and contributed to the review and editing of the article. FOV analyzed immunohistopathology data. SV contributed by performing and analyzing confocal microscopy results. PC contributed to the conception of new experiments, analyzed the data, and contributed to the review and editing of the article. AGD discussed and analyzed the data. FJO conceived the project, analyzed the data, and contributed to writing the article.

Data availability statement

The transcriptomics data presented in this study are available in the supplementary material; they have been deposited in the National Center for Biotechnology Information (NCBI) and can be accessed via BioProject ID PRJNA769662 (https://www.ncbi.nlm.nih.gov/bioproject/PRJNA769662).

References

1. Viallard C, Larrivée B. Tumor angiogenesis and vascular normalization: alternative therapeutic targets. *Angiogenesis* 2017; **20:** 409–426.
2. Folkman J. Tumor angiogenesis: therapeutic implications. *N Engl J Med* 1971; **285:** 1182–1186.
3. Jayson GC, Kerbel R, Ellis LM, *et al*. Antiangiogenic therapy in oncology: current status and future directions. *Lancet* 2016; **388:** 518–529.
4. Maniotis AJ, Folberg R, Hess A, *et al*. Vascular channel formation by human melanoma cells *in vivo* and *in vitro*: vasculogenic mimicry. *Am J Pathol* 1999; **155:** 739–752.
5. Delgado-Bellido D, Serrano-Saenz S, Fernández-Cortés M, *et al*. Vasculogenic mimicry signaling revisited: focus on non-vascular VE-cadherin. *Mol Cancer* 2017; **16:** 65.
6. Yang JP, Liao YD, Mai DM, *et al*. Tumor vasculogenic mimicry predicts poor prognosis in cancer patients: a meta-analysis. *Angiogenesis* 2016; **19:** 191–200.
7. Schito L, Semenza GL. Hypoxia-inducible factors: master regulators of cancer progression. *Trends Cancer* 2016; **2:** 758–770.
8. Martí JM, Fernández-Cortés M, Serrano-Sáenz S, *et al*. The multifactorial role of PARP-1 in tumor microenvironment. *Cancers (Basel)* 2020; **12:** 739.
9. Gupte R, Liu Z, Kraus WL. PARPs and ADP-ribosylation: recent advances linking molecular functions to biological outcomes. *Genes Dev* 2017; **31:** 101–126.
10. Martí JM, Garcia-Diaz A, Delgado-Bellido D, *et al*. Selective modulation by PARP-1 of HIF-1α-recruitment to chromatin during hypoxia is required for tumor adaptation to hypoxic conditions. *Redox Biol* 2021; **41:** 101885.
11. Gonzalez-Flores A, Aguilar-Quesada R, Siles E, *et al*. Interaction between PARP-1 and HIF-2α in the hypoxic response. *Oncogene* 2014; **33:** 891–898.
12. Yu X, Ambrosini G, Roszik J, *et al*. Genetic analysis of the 'uveal melanoma' C918 cell line reveals atypical BRAF and common KRAS mutations and single tandem repeat profile identical to the cutaneous melanoma C8161 cell line. *Pigment Cell Melanoma Res* 2015; **28:** 357–359.
13. Andrés-León E, Núñez-Torres R, Rojas AM. miARma-seq: a comprehensive tool for miRNA, mRNA and circRNA analysis. *Sci Rep* 2016; **6:** 25749.
14. Andrews S. FastQC: a quality control tool for high throughput sequence data. Babraham Bioinformatics, 2010. [Accessed October 2017]. Available from: http://www.bioinformatics.babraham.ac.uk/projects/fastqc
15. Li H. Seqtk: toolkit for processing sequences in FASTA/Q formats. 2012. [Accessed October 2017]. Available from: https://github.com/lh3/seqtk.
16. Kim D, Langmead B, Salzberg SL. HISAT: a fast spliced aligner with low memory requirements. *Nat Methods* 2015; **12:** 357–360.
17. Liao Y, Smyth GK, Shi W. featureCounts: an efficient general purpose program for assigning sequence reads to genomic features. *Bioinformatics* 2014; **30:** 923–930.
18. Yu G, Wang LG, Han Y, *et al*. clusterProfiler: an R package for comparing biological themes among gene clusters. *OMICS* 2012; **16:** 284–287.
19. Subramanian A, Tamayo P, Mootha VK, *et al*. Gene set enrichment analysis: a knowledge-based approach for interpreting genome-wide expression profiles. *Proc Natl Acad Sci U S A* 2005; **102:** 15545–15550.
20. Schindelin J, Arganda-Carreras I, Frise E, *et al*. Fiji: an open-source platform for biological-image analysis. *Nat Methods* 2012; **9:** 676–682.
21. Delgado-Bellido D, Fernández-Cortés M, Rodríguez MI, *et al*. VE-cadherin promotes vasculogenic mimicry by modulating kaiso-dependent gene expression. *Cell Death Differ* 2019; **26:** 348–361.
22. Takase H, Matsumoto K, Yamadera R, *et al*. Genome-wide identification of endothelial cell-enriched genes in the mouse embryo. *Blood* 2012; **120:** 914–923.
23. Strilić B, Kučera T, Eglinger J, *et al*. The molecular basis of vascular lumen formation in the developing mouse aorta. *Dev Cell* 2009; **17:** 505–515.
24. Lindahl P, Johansson BR, Levéen P, *et al*. Pericyte loss and microaneurysm formation in PDGF-B-deficient mice. *Science* 1997; **277:** 242–245.
25. Hess AR, Seftor EA, Gardner LMG, *et al*. Molecular regulation of tumor cell vasculogenic mimicry by tyrosine phosphorylation: role of epithelial cell kinase (Eck/EphA2). *Cancer Res* 2001; **61:** 3250–3255.
26. Gaynor R, Irie R, Morton D, *et al*. S100 protein: a marker for human malignant melanomas? *Lancet* 1981; **317:** 869–871.
27. Schlingemann RO, Rietveld FJR, Kwaspen F, *et al*. Differential expression of markers for endothelial cells, pericytes, and basal lamina in the microvasculature of tumors and granulation tissue. *Am J Pathol* 1991; **138:** 1335–1347.

28. Thijssen VL, Paulis YW, Nowak-Sliwinska P, *et al*. Targeting PDGF-mediated recruitment of pericytes blocks vascular mimicry and tumor growth. *J Pathol* 2018; **246:** 447–458.
29. Schnegg CI, Yang MH, Ghosh SK, *et al*. Induction of vasculogenic mimicry overrides VEGF-A silencing and enriches stem-like cancer cells in melanoma. *Cancer Res* 2015; **75:** 1682–1690.
30. Xu Y, Li Q, Li X-Y, *et al*. Short-term anti-vascular endothelial growth factor treatment elicits vasculogenic mimicry formation of tumors to accelerate metastasis. *J Exp Clin Cancer Res* 2012; **31:** 16.
31. Fernández-Cortés M, Andrés-León E, Oliver FJ. The PARP inhibitor olaparib modulates the transcriptional regulatory networks of long non-coding RNAs during vasculogenic mimicry. *Cell* 2020; **9:** 2690.
32. Legrand AJ, Choul-Li S, Spriet C, *et al*. The level of Ets-1 protein is regulated by poly(ADP-ribose) polymerase-1 (PARP-1) in cancer cells to prevent DNA damage. *PLoS One* 2013; **8:** e55883.
33. Oda N, Ma A, Sato Y. ETS-1 converts endothelial cells to the angiogenic phenotype by inducing the expression of matrix metalloproteinases and integrin β_3. *J Cell Physiol* 1999; **178:** 121–132.
34. Lelièvre E, Mattot V, Huber P, *et al*. ETS1 lowers capillary endothelial cell density at confluence and induces the expression of VE-cadherin. *Oncogene* 2000; **19:** 2438–2446.
35. Wei G, Srinivasan R, Cantemir-Stone CZ, *et al*. *Ets1* and *Ets2* are required for endothelial cell survival during embryonic angiogenesis. *Blood* 2009; **114:** 1123–1130.
36. Chen J, Fu Y, Day DS, *et al*. VEGF amplifies transcription through ETS1 acetylation to enable angiogenesis. *Nat Commun* 2017; **8:** 383.
37. Seftor EA, Meltzer PS, Schatteman GC, *et al*. Expression of multiple molecular phenotypes by aggressive melanoma tumor cells: role in vasculogenic mimicry. *Crit Rev Oncol Hematol* 2002; **44:** 17–27.
38. Riedel T, Cavin S, Van Den Bergh H, *et al*. Chemo-manipulation of tumor blood vessels by a metal-based anticancer complex enhances antitumor therapy. *Sci Rep* 2018; **8:** 10263.
39. Martin JD, Seano G, Jain RK. Normalizing function of tumor vessels: Progress, opportunities, and challenges. *Annu Rev Physiol* 2019; **81:** 505–534.

SUPPLEMENTARY MATERIAL ONLINE

Figure S1. PARP inhibition and hypoxia regulate the expression of hundreds of genes during uveal melanoma tube formation

Figure S2. The combination of PARP inhibition plus hypoxia enriches vasculogenic gene expression in VM^+ uveal melanoma cells during tube formation

Figure S3. PARP inhibition and hypoxia modulate tube formation by cutaneous melanoma cells

Figure S4. PARP inhibition and hypoxia modulate tube formation by endothelial cells

Figure S5. siRNA-mediated knockdown of PDGFB expression in Mum2B cells

Figure S6. Generation of human uveal melanoma xenografts

Figure S7. PARP inhibition increases pericyte recruitment to endothelial vessels in VM^- tumors *in vivo*

Table S1. Whole-transcriptome profiling of Mum2B cells during tube formation

Table S2. Gene set enrichment analysis and gene ontology terms related to vascular function after olaparib and hypoxia